Ion Temperature and Toroidal Velocity Edge Transport Barriers in KSTAR

Won-Ha Ko[1,2], S.H. Ko[3], J.M. Kwon[3], P.H. Diamond[3,4], K. Ida[5], Y.M. Jeon[1], J.H. Lee[1,2], S.W. Yoon[1], and J.G. Kwak[1]

[1]National Fusion Research Institute, Daejeon, Korea;

[2]Korea University of Science and Technology (UST), Daejeon, Korea

[3]WCI Center for Fusion Theory, National Fusion Research Institute, Daejeon, Korea;

[4]CMTFO and CASS, University of California, San Diego, USA;

[5]National Institute for Fusion Science, Toki, Japan

E-mail contact of main author: whko@nfri.re.kr

Abstract. The structure and evolution of ion temperature (T_i) and toroidal rotation (V_ϕ) profile have been investigated in NBI-heated KSTAR H-mode plasmas, both without and with RMP. A clear disparity between the width of the V_ϕ-pedestal and that of the T_i-pedestal was observed. Also, it was found that there exist close correlation and weak relative hysteresis between the pedestal ∇V_ϕ and ∇T_i during both L→H and H→L transitions. During the L→H transition, the V_ϕ-pedestal is observed to form ahead of the T_i-pedestal, and build inward from the separatrix. Linear gyrokinetic stability analysis of these KSTAR profiles was performed. The results indicate that parallel velocity shear is a relevant drive for pedestal turbulence and transport. This was largely ignored in previous studies of the pedestal micro-stability. Pedestal ion temperature and rotation profiles were also measured during ELM suppression experiments on KSTAR using an n=1 RMP. It was found that the top values of the ion temperature and toroidal rotation pedestal drop with RMPs when ELMs are suppressed.

1. Introduction

$E \times B$ shear is important for stabilizing micro- and macro-instabilities in tokamak plasmas. Neutral beam is injected to the plasmas as an external momentum source to produce and control plasma rotation, which contributes to the generation of the $E \times B$ shearing. Pedestal rotation profiles are of great importance for ITER, in the contexts of confinement enhancement, understanding the intrinsic torque in H-mode, and the plasma response to ELMs and to ELM suppression techniques [1-5].

Most previous studies of H-mode profiles have focused on electron density and temperature profile structure, and more attention should be devoted to the study of V_ϕ pedestal structure. We note that extensive studies on the T_i and V_ϕ profiles have been performed on other machines such as AUG, DIII-D and C-Mod [6-9]. However, despite the plethora of data concerning density and temperature pedestals, rather little information concerning toroidal rotation profiles is available. In this paper, we present detailed Charge Exchange Spectroscopy (CES) measurements [10,11] and studies of V_ϕ- and T_i-pedestal

profile structure and evolution across the L→H and H→L transitions and during ELMs. We also investigate ∇V_ϕ as a drive of pedestal micro-instability.

The conventional neoclassical theory [12] predicts that the T_i-pedestal width, Δ_i^{ped} should be broader and the V_ϕ-pedestal width, Δ_ϕ^{ped} (i.e. $\Delta_i^{ped} > \Delta_\phi^{ped}$), since the neoclassical ion thermal diffusivity χ_i^{neo} in the pedestal should exceed the residual turbulent viscosity in H-mode and the scale of Δ_i^{ped} should exceed the poloidal ion gyro-radius $\rho_{\theta i}$. However, KSTAR results show $\Delta_\phi^{ped} > \Delta_i^{ped}$ from the experiments, which differ from the conventional neoclassical picture. In this work, we present detailed gyrokinetic analyses of these profiles and investigate the role of the V_ϕ-pedestal in the micro-instability.

ELM suppression experiments were performed with an n=1 RMP using the segmented in-vessel control coil (IVCC) system on KSTAR [13]. We also report detailed measurements of pedestal ion temperature and rotation profiles during the ELM suppression phase.

The remainder of this paper is organized as follows. We introduce the experimental setup in KSTAR in section 2. Section 3 gives the main experimental results, which include pedestal structure, evolution, transition hysteresis both without and with RMP, and rotation evolution during RMP operation. Gyrokinetic stability analyses using measured profiles are also presented in this section. Section 4 gives summary and future plans.

2. Experimental Setup

The CES system on KSTAR was installed to obtain the ion temperature and toroidal rotation velocity profiles [10, 11]. CES is used to measure the carbon VI spectral line at 529.05 nm. The measurement of the ion temperature profiles has been used to classify L- and H-mode KSTAR plasmas [14, 15].

The KSTAR CES system consists of a spectroscopic system looking at the KSTAR neutral beam which is modulated at 5 Hz to provide ion temperature and toroidal rotation profile measurement [16, 17]. There are 32 channels installed in the spectrometer, which are focused on the plasma region from the major radius of 1.8 m to 2.3 m. The space between fibers is about 5 mm in plasma edge at the focal point, while the space between the channels in core is 50 mm. The spatial resolution including effects due to the beam geometry and divergence is near 5 mm in edge and less than 20 mm in core region. The entrance slit was fully open and we can measure the full fiber (ϕ=0.4mm) for all channels. The wavelength calibration has been conducted with a Ne I spectral lamp as a calibration source [11]. The measured instrumental width and dispersion of Ne lamp are 0.28 nm and 0.72 nm/mm, respectively. The high throughput spectrometer lent from NIFS [18, 19] provides us a good spatial-temporal resolution of the measure profiles. The time and spatial resolution of the measurements at the plasma edge are 100 Hz and 5 mm, respectively.

3. Experimental Results

A. Pedestal Structure during L→H Transition

Measurements of ion temperature and toroidal rotation velocity profiles have been conducted for a KSTAR discharge with shot number #5681. Figure 1 shows the measured profiles at the times of 2.015 and 2.435 sec, in L-mode (black) and H-mode (red), respectively. The plasma current is 630 kA and the line integrated density is 2.5×10^{19} m^{-2}. 1.44 MW NBI with 95 keV was injected, and NBI heated H-mode plasma was achieved after 2.0 sec. NBI

was modulated with 5Hz frequency and 95% duty cycle as 190 ms on and 10 ms off phase, which was used for a background subtraction. The signal integration time of CCD is 5.5 ms and the time window of the subtraction can be selected from beam power data in analysis program. The major radii of the last closed flux surface is around 2.3 m and 2.25m in the L- and H-mode phase, respectively.

As the figure shows, in the L-mode case, the ion temperature increases almost linearly from the very plasma edge, while the toroidal rotation shows a modest pedestal structure. After the L→H transition, the ion temperature profile develops a strong edge gradient due to transport barrier formation and the core temperature increases correspondingly. The toroidal rotation increases over the whole region in the H-mode plasma, as compared to that for the L-mode state.

The evident disparity between the width of the V_ϕ-pedestal ($\Delta_\phi^{ped} \sim 5$ cm) and that of the T_i pedestal ($\Delta_i^{ped} \sim 2\ cm$) in the H-mode state is immediately noticeable. As mentioned in the introduction, the conventional neoclassical picture says the T_i pedestal should be broader, since the residual turbulence in H-mode is expected to drive quite a modest χ_ϕ, while the collisional viscosity χ_ϕ^{neo} is almost negligible compared to the neoclassical ion heat diffusivity χ_i^{neo} i.e. $\chi_i^{neo} \gg \chi_\phi^{neo}$. We note that the poloidal ion gyro-radius $\rho_{\theta i}$ is a natural minimal scale for the neoclassically regulated pedestal. The experimental parameters give $\rho_{\theta i} \sim$ 1.8 cm in the pedestal, which is very close to the measured width, $\Delta_i^{ped} \sim 2$ cm. Thus, we expect the ion thermal diffusivity χ_i in the pedestal to significantly exceed χ_ϕ so that the T_i profile should be broader, which is in clear contrast with the KSTAR experimental observation of $\Delta_\phi^{ped} > \Delta_i^{ped}$. For the comparison of pedestals of profiles, we applied the modified hyperbolic tangent function to extract pedestal parameters such as height and width [20]. If the pedestal transport is only governed by the collisional processes, the pedestal widths in steady state will be determined by the corresponding neoclassical transport coefficients. Since $\chi_i^{neo} \gg \chi_\phi^{neo}$, it is naturally expected that the gradients will show the opposite trend i.e. $\nabla V_\phi \gg \nabla T_i$. But what we observe from the experiment is $\nabla T_i \gg \nabla V_\phi$ in the pedestals. We also obtained the evolutions of V_ϕ and T_i pedestal during the L→H transition. The high spatial resolution measurements of the profiles clearly reveal the differences of V_ϕ and T_i evolution in the edge region as shown on Figure 2 and 3. Figure 3 shows core and edge parameters and the gray line is L to H transition point in which a big drop of D_α signal appears. The edge and core parameters are obtained from the same radial position for T_i and V_ϕ. In this figure, the V_ϕ pedestal is observed to form ahead of the T_i pedestal as the rapid increase of the V_ϕ pedestal top shows (the red dotted line in the 3rd panel of figure 3).

Interestingly, we can find the same trend in the correlation between ∇T_i and ∇V_ϕ during the LH transition in figure 4. At the beginning of the transition, which is represented by the black dots, the curve is elongated to the vertical direction. This also implies that ∇V_ϕ increases first during the transition. This observation is consistent with the expectation that toroidal momentum transport is effectively governed by turbulence only, while neoclassical ion thermal transport plays a significant role in T_i profile evolution. Thus, V_ϕ should and indeed does react more rapidly to the suppression of turbulence at the L→H transition than T_i does. In a related and consistent vein, we observe that V_ϕ also responds faster and more strongly to an ELM than T_i does as shown in Figure 5. The rotation pedestal clearly decreased during ELM crash and it was recovered after the ELM crash while it is difficult to see clear drop in ion temperature pedestal during ELM crash in figure 5.

Figure 4 shows the evolutions of the T_i and V_ϕ gradients which are maximum values in the edge pedestal during the L→H and H→L transitions. Due to the limited time resolution of the CES measurement, we have only a few data points in the curve during the transitions. However, it is notable that the curve exhibits a trend of weak relative hysteresis between ∇T_i and ∇V_ϕ [17]. This suggests that a single transport process controls both channels during the transitions. The correlation in gradients, which is directly related to the driving fluxes, is more revealing than the correlation in the quantities themselves. We also remark that pedestal profiles are effectively unchanged by the addition of 400 kW of ECH on axis, while core profiles are modified significantly [21].

B. Rotation for Stored Energy and Modeling during LH transition

Figure 6 shows a plot of $V_\phi(0)$ and V_ϕ at the pedestal top vs $\Delta W/I_P$ (ΔW is the stored energy change across the L→H transition, and I_P is total plasma current). A linear scaling relation is apparent for both $V_\phi(0)$ and the pedestal top V_ϕ before $\Delta W/I_P$ reaches 0.15. Note that this resembles the 'Rice scaling', and gives the relation between the increase of core and pedestal V_ϕ and the increase in stored energy. However, in contrast to the usual 'Rice scaling' trend [22], this variation describes a plasma with co-NBI torque. The pedestal top V_ϕ saturates after $\Delta W/I_P$ exceeds 0.15. The unfavorable scaling of $V_\phi(0)$ with I_P is noteworthy, because other plasma confinements usually show favorable scaling with the plasma current. So, it is interesting to check whether we can recover a similar scaling of $V_\phi(0)$ for other physical quantities which are in favorable scaling with I_P. Figure 7 shows such an example and we can see a clear linear proportionality between $\Delta W/I_P$ and $\Delta W/n_e$, which implies $V_\phi(0) \propto \Delta W/n_e$. The question of how such a trend can apply to a co-NBI H-mode is addressed in the following paragraph.

A simple 0D model illustrates how the above trend can appear for co-NBI rotation scaling. The key point is that development of the edge transport barrier H-mode results in both enhanced momentum confinement (i.e. an increase in τ_ϕ the momentum confinement time) and the development of a significant intrinsic torque, situated in the edge pedestal. For co-NBI and intrinsic co-torque, the two effects add. Thus, for mean rotation $\bar{V}_\phi$, we have

$$(1a) \quad \partial_t \bar{V}_\phi + \frac{\bar{V}_\phi}{\tau_\phi} = T_b + T_{intr} \ ,$$

where:

$$(1b) \quad T_{intr} = -\partial_r \Pi_{resid} \sim \frac{\chi_\phi V_{th}}{L_{ped} L_{sym}} \ .$$

Here, T_b is the beam torque, T_{intr} is the intrinsic torque, Π_{resid} is the residual stress, L_{ped} represents T_i pedestal scale length and L_{sym} is the scale length of the underlying symmetry breaking (i.e. the scale length of the strong $E \times B$ shear region) [23]. In practice, $L_{ped} \sim L_{sym}$. Now, at the L→H transition, τ_ϕ increases and T_{intr} increases.

Thus:

$$(2) \quad \Delta \bar{V}_\phi \cong \left(\tau_\phi^H - \tau_\phi^L\right) T_b + \left(\tau_\phi^H T_{intr}^H\right)$$

Experimentally, it is known that the intrinsic torque is proportional to the ion temperature gradient in the pedestal [19,22]. Considering the modest temperature gradient in the L-mode, we neglect the pedestal intrinsic torque in the L-mode and we take $1/\tau_\phi^L \sim \chi_\phi/a^2$,

$1/\tau_\phi^H \sim (\chi_\phi/a^2)F(V'_E/\omega_0)$,and $\tau_\phi^H \chi_\phi^H = \tau_\phi^L \chi_\phi^L$ where $F(V'_E/\omega_0) \sim 1/(1 + V'^2_E/\omega_0^2)$ is typical form factor for χ_ϕ reduction in H-mode, due to enhanced $E \times B$ shearing. Here a denotes the minor radius. We then obtain the increment in mean rotation $\Delta\bar{V}_\phi$:

$$(3) \quad \Delta\bar{V}_\phi \cong \tau_\phi^L \left(\frac{V'^2_E}{\omega_0^2}\right) T_b + \tau_\phi^L \left(\frac{V_{thi}}{L_{ped}} \frac{\chi_\phi^L}{L_{sym}}\right),$$

Note that the two contributions are additive. Since the main symmetry breaking mechanism is the shearing of the equilibrium radial electric field in the pedestal, which can be estimated by the neoclassical radial force balance, we can set $L_{sym} \sim L_{ped} \sim L_{V'_E}$ (the $E \times B$ shear scale length). It follows that;

$$(4a) \quad \Delta\bar{V}_\phi \sim \left(\frac{\tau_\phi^L}{L_{ped}^2}\right)\left[\left(\frac{V'_E}{\omega_0}\right)^2 L_{ped}^2 T_b + V_{thi} \chi_\phi^L\right]$$

Finally, taking $\chi_\phi^L \sim \chi_i^L$ and $\tau_\phi^L \sim \tau_i^L$, using $Q_i = \chi_i \nabla T_i$, and taking $L_{Ti} \sim a$ for L-mode, we have;

$$(4b) \quad \Delta\bar{V}_\phi \sim \left(\frac{\tau_\phi^L}{L_{ped}^2}\right)\left[\left(\frac{V'_E}{\omega_0}\right)^2 L_{ped}^2 T_b + \frac{V_{thi} a}{T_i} Q_i\right].$$

We see that the co-directionality of NBI and intrinsic torques, the common length scale dependence of L_{ped}^{-2}, and the proportionality $T_b \propto Q_i$ for NBI heating together support the scaling form for the increment $\Delta\bar{V}_\phi$. For purely intrinsic torque, we have $\Delta\bar{V}_\phi \sim (\tau_\phi^L/L_{ped}^2)[(V_{thi} a/T_i)Q_i]$, which is consistent with the heat engine model of intrinsic rotation (i.e. note $\Delta\bar{V}_\phi \propto Q_i$) [24-27]. Note also that the central parameter which determines the relative contributions to $\Delta\bar{V}_\phi$ is Q_i/T_b or, equivalently, P_i/T_b, the ratio of ion power input to torque [28].

C. Gyrokinetic analysis of micro-stability in pedestal: ∇V_ϕ-driven shear flow instability

The experimental observations of the steep V_ϕ pedestal and the trend $\Delta_\phi^{ped} > \Delta_i^{ped}$ strongly suggest that there should be instabilities regulating the toroidal rotation pedestal. Also, it is interesting to notice that the V_ϕ pedestal saturates for large $\Delta W/I_P$, while $V_\phi(0)$ continues to increase as shown in Figure 6. This may be due to the instabilities enhanced by the steep ∇V_ϕ, which are limiting the pedestal. In this subsection, we present a detailed analysis of micro-stabilities including the toroidal rotation pedestal.

Generally, the parallel shear flow instability (PSFI) can be driven by a strong ∇V_ϕ and mediate anomalous momentum transport. PSFI is stabilized by density gradient and its key control parameters are $\eta_i = L_n/L_{T_i}$ and $\nabla V_\parallel$, where L_n and L_{T_i} represent the gradient length scale of density and ion temperature profile, respectively. $V_\parallel$ denotes the component of ion flow velocity parallel to equilibrium magnetic field, and we set $\nabla V_\parallel \approx \nabla V_\phi$, since $B_\phi \approx B$ in the KSTAR experiments.

We employed GYRO code [29] for local linear analysis of micro-instability using measured pedestal profiles of a KSTAR H-mode experiment (shot number #8762), which exhibits very similar characteristics of T_i and V_ϕ pedestal profile with those of #5681 as shown in figure 1 and 8, and yet provides more complete information for the micro-instability analysis. In the analysis, the newest version GYRO is used with the kinetic electron responses [30-31].

Figure 8 shows all profiles from discharge #8762 used in the GYRO analysis instead of those from discharge #5681 as shown in figure 1. Figure 9(a) and 9(b) show the calculated instabilities in the pedestal. In these analyses, we optionally switched on and off the ∇V_ϕ-driving term to clearly see its effects. Without the ∇V_ϕ-drive, the instabilities are propagating to the ion and electron diamagnetic direction according to the wave length $k_\theta \rho_s$, which indicate the excitations of ion temperature gradient (ITG) mode and trapped electron (TEM) mode depending on the wave length. Here, k_θ is the poloidal wave number and $\rho_s = \sqrt{m_i T_e / eB}$. Dominant instabilities are ITG, which are excited in the lower mode numbers ($k_\theta \rho_s < 0.6$) and have the largest growth rate.

Dominant instabilities are ITG, which are excited in the lower mode numbers ($k_\theta \rho_s < 0.6$) and have the largest growth rate. TEM modes appear for higher mode numbers ($k_\theta \rho_s > 0.6$) when the ∇V_ϕ-drive is not included in the analysis. When we turn on the ∇V_ϕ-drive, it is found that all instabilities in the range of the mode numbers are propagating toward the ion direction with enhanced growth rates. This suggests that ∇V_ϕ-driven PSFI does impact the pedestal stability.

We also performed a sensitivity study of the micro-instabilities on density gradient by varying the gradient value (a/L_{n_e}) from -50% to +50% of the experimentally measured level. Figure 10(a) and 10(b) show that the instabilities become more stabilized for steeper density gradients as expected from the dependence of PFSI on the density gradient.

The GYRO analysis results indicate that the micro-instabilities enhanced by strong parallel shear flow can affect the momentum transport in the rotation pedestal, which was largely ignored in the previous studies of the pedestal micro-instability [32]. More detailed and comprehensive analysis of pedestal transport and micro-instability are ongoing, and will be reported in future works.

D. **Pedestal Rotation with and without RMP**

Resonant magnetic field perturbation (RMP) is actively employed in ELM control experiment [33-38]. Generally, RMP can change pedestal transport and regulate pedestal profiles to stay below the thresholds for the peeling-ballooning instabilities. The effects of RMP on pedestal transport are important subject to study for better understanding of the underlying physical mechanisms of ELM suppression by RMP.

Pedestal rotation profiles have been measured during ELM suppression experiments using an n=1 and n=2 RMP on KSTAR [13, 33]. The IVCC system of KSTAR was used, which can apply n=1, 2 RMPs with various parities. We obtained an ELM suppression state by applying n=1 RMP with the coil current $I_C = 1.8\ kA/t$ and 90 phasing configuration. Figure 11 shows unambiguously that the V_ϕ and T_i pedestal top drop during the ELM suppression. In this figure, the magenta curves show the profiles in an inter-ELM period without RMP. When the RMP coil is turned on, both the pedestals and its widths decrease. The decrease of the pedestal widths mainly comes from the drop of the pedestal though the pedestal slopes show modest changes. It is notable that the rotation pedestal responds more quickly and shows larger reduction ($> 30\%$) as compared to the ion temperature pedestal. Similar profile changes by RMP were also reported in KSTAR [33]. Generally, V_ϕ decreases during ELM suppression but recovers its pre-suppression value once RMP is turned off and ELMs reappear as shown in figure 12.

In KSTAR, there are certain windows of plasma parameters to achieve ELM suppression either using n=1 or n=2 RMP. Out of these windows, only the reduction of the pedestal rotation appears due to the magnetic braking introduced by RMP. The amplitude of the reduction depends on the details of RMP configurations. More generally, RMP causes the damping of toroidal rotation in both L- and H-mode. We can clearly see the magnetic braking effect on the toroidal rotation. More detailed and comprehensive analysis of the magnetic braking effect is ongoing, and will be reported in future works.

4. Summary and Future Plans

We studied the structure and evolution of T_i and V_ϕ profiles in co-NBI heated plasmas on KSTAR using CES with 5 mm spatial resolution in edge and 10 ms time resolution. Both T_i and V_ϕ show a clear pedestal structure in H-mode, while only V_ϕ shows pedestal structure in L-mode. In H-mode plasmas, we observed the pedestal width inequality $\Delta_\phi^{ped} > \Delta_i^{ped}$, which is contrary to the conventional wisdom $\Delta_i^{ped} > \Delta_\phi^{ped}$. We note that local turbulences involved in LH transition have much faster time scales than the CES time resolution. Therefore, fluctuation diagnostics should be employed to fully resolve the detailed dynamics of the transition and pedestal formation. However, slower transport changes and resulting pedestal build-ups can be clearly captured by the CES measurement. Figure 3 shows the temporal evolutions of the ion temperature and rotation pedestal during the transition, and we can find that the V_ϕ responds faster and more strongly to the L-H transitions than T_i does. From linear micro-stability analyses of the measured profiles, we found that ∇V_ϕ is a relevant driving force of micro-instability in the pedestal, which can regulate the pedestal and gradient. Hysteresis appears in both T_i and V_ϕ, and here is a weak relative hysteresis between ∇T_i and ∇V_ϕ. The V_ϕ pedestal top value drops and Δ_ϕ^{ped} decreases during ELM suppression by RMP. V_ϕ pedestal structure is recovered once the ELM reappears by turning off RMP.

It is uncertain whether this increase of the toroidal rotation velocity is due to the large radial gradient of the velocity, even though there appears to be also a momentum transport barrier in the edge region, like that for temperature. Since the carbon rotation is expected to be much different from the main ion velocity in the edge region, knowledge of the main ion velocity profile is necessary for the correct momentum transport analysis [19]. Such detailed transport analysis is left to the future, since the estimation of the main ion velocity and the measurement of the radial electric field are not yet available.

Ongoing work is concerned primarily with measurement of pedestal density during L→H and H→L transition, the analysis of fluctuation measurements during the transition using BES, and more detailed transport analyzes related to the evolution of intrinsic torque during L→H and H→L transitions. We also plan an investigation of residual momentum transport in the pedestal using a comprehensive analysis of pedestal micro-stability. A study of parallel shear flow instability effects in the H-mode V_ϕ pedestal is of particular interest, and is ongoing. This issue is also relevant to the dynamics of QH-mode. A poloidal CES system or Doppler backscattering diagnostic is required for a complete study of V_θ and E_r during transitions.

Reference

[1]   FIELDING, S. J. et al., Europhys. Conf. Abstr. **25A**, 1825(2001).

[2]   EVANS, T. E. et al., Phys. Rev. Lett. **92**, 235003 (2004).

[3]   CANIK, J. M. et al., Phys. Rev. Lett. **104**, 045001 (2010).

[4]   LIANG, Y. et al., Phys. Rev. Lett. **98**, 265004 (2007).

[5]   SUTTROP, W. et al., Phys. Rev. Lett. 106, 225004 (2011).

[6]   PUTTERICH, T., et. al., Phys. Rev. Lett. **102**, 025001 (2009)

[7]   VIEZZER, E., et. al., Plasma Phys. Control. Fusion 55 124037 (2013)

[8]   WADE, M. R., et. al., Nucl. Fusion 55, 023002 (2015).

[9]   RICE, J. E., et. al., Phys. Rev. Lett. 111, 125003(2013).

[10]   KO, W.H. *et al*., IEEE. Trans. Plasma Sci. 38, 996 (2010).

[11]   KO, W.H., LEE, H., SEO, D., *et al*., Rev. Sci. Instrum. **81** 10D740 (2010).

[12]   DIAMOND, P.H., et. al., Nucl. Fusion. 49, 045002(2009).

[13]   JEON, Y. M. *et al*., Phys. Rev. Lett. 109, 035004 (2012).

[14]   YOON, S.W. *et al*., Nucl. Fusion. 51, 113009 (2011).

[15]   AHN, J. W., *et al*., Nucl. Fusion. 52, 114001 (2012).

[16]   LEE, H. *et al*., Rev. Sci. Instrum. 82, 063510 (2011).

[17]   KO, W.H. *et al*., 39th EPS and 16th ICPP, Stockholm, Sweden, 2-6 July (2012).

[18]   YOSHINUMA, M., IDA K., *et al*., Fus. Sci. Tech. 58, 375 (2010).

[19]   IDA, K. , et. al., Nucl. Fusion 50, 064007 (2010).

[20]   GARLSTROM, T. N., et. al., Nucl. Fusion., 39, 1941 (1999)

[21]   SHI Y.J., et. al., Nucl. Fusion 53, 113031(2013).

[22]   RICE, J.E., et al., Phys. Rev. Lett. 106, 215001(2011)

[23]   DIAMOND, P.H., et. al., Phys. Plamsas 15, 012303(2008).

[24]   KOSUGA, Y. et al., Phys. Plasmas 17, 102313(2010).

[25]   SOLOMON, W. M., et. al., Nucl. Fusion 51, 073010 (2011)

[26]   MCDERMOTT, R. M., et. al., Nucl. Fusion 54, 043009 (2014)

[27]   HOWARD, N. T., et. al., Plasma Phys. Control. Fusion 56 124004 (2014)

[28]   HUBBARD, A. E., et. Al., Plasma Phys. Control. Fusion 44, A359 (2002).

[29]   CANDY, J., et. al., J. Comput. Phys. 186, 545(2003).

[30]   SNYDER, P. B., et. al., Phys. Plasmas, 16, 056118 (2009)

[31]   SNYDER, P. B., et. al. Nucl. Fusion, 51, 103016 (2011)

[32] WANG, E., et. al., Nucl. Fusion 52, 103015(2012).

[33] KO, W.H., *et al.*, Rev. Sci. Instrum. **85** 11E413 (2014).

[34] EVANS, T. E., et al., Nucl. Fusion **48**, 024002(2008)

[35] LIANG, Y., et al., Nucl. Fusion **51**, 073001 (2011)

[36] KIRK, A., et al., Nucl. Fusion 50, 034008 (2010)

[37] VIEZZER, E., et. al., Nucl. Fusion 53 (2013) 053005

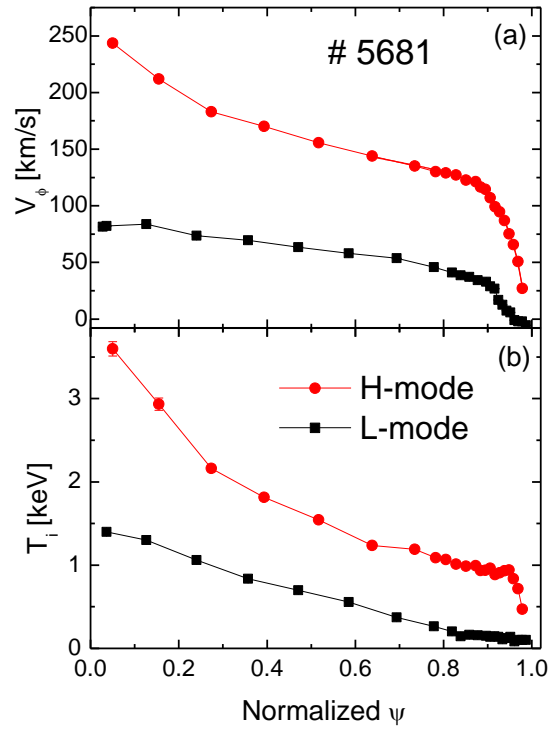[38] MORDIJCK, S., Nucl. Fusion 54 (2014) 082003

Figures

Figure 1. Carbon impurity toroidal rotation (a) and ion temperature (b) profiles for L(black squre) and H mode(red circle). Note that the width of the V_ϕ pedestal in H-mode exceeds that of the T_i pedestal.
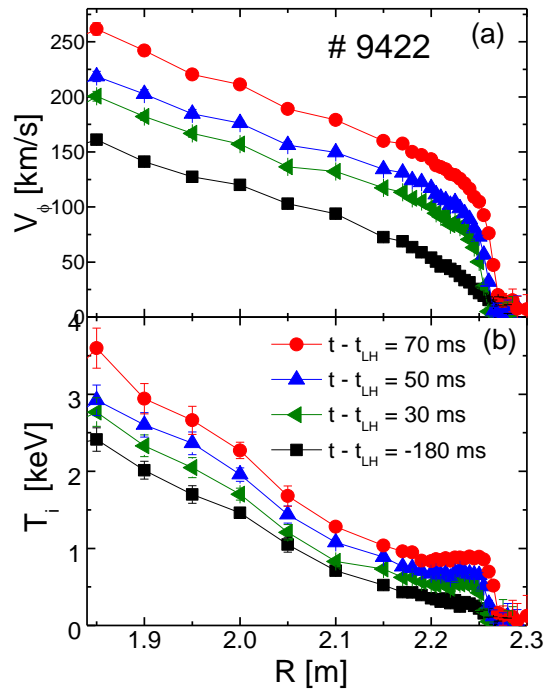
Figure 2. Profiles evolution of (a) toroidal rotation and (b) ion temperature from carbon impurity line at the L$\rightarrow$ H transition.
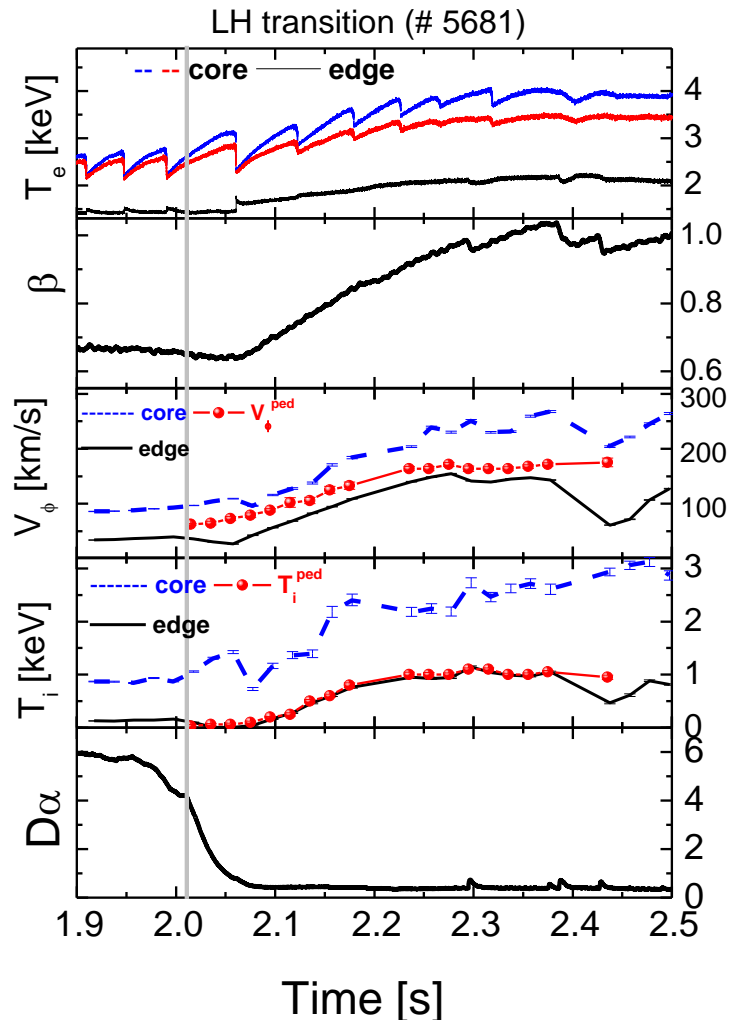
Figure 3. T_e from electron cyclotron emission radiometer, plasma beta, carbon impurity rotation, ion temperature and D_a and the pedestal evolution of between V_ϕ and T_i during L to H transition.
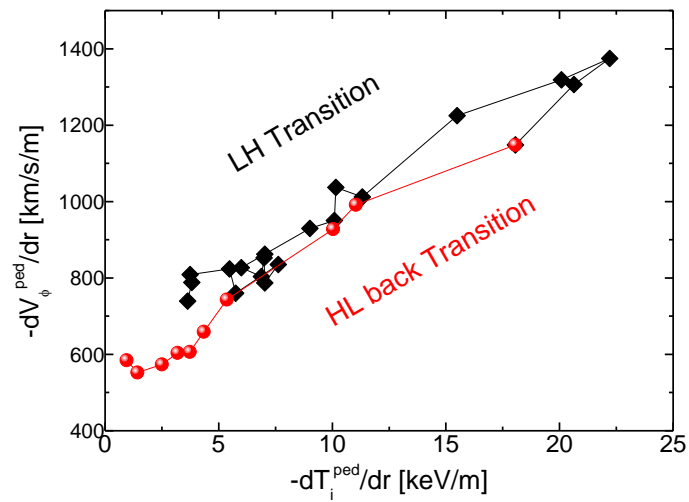
Figure 4. Correlation between pedestal ∇V_ϕ and ∇T_i during L→H transition (black squares) and H→L back transition (red circles).
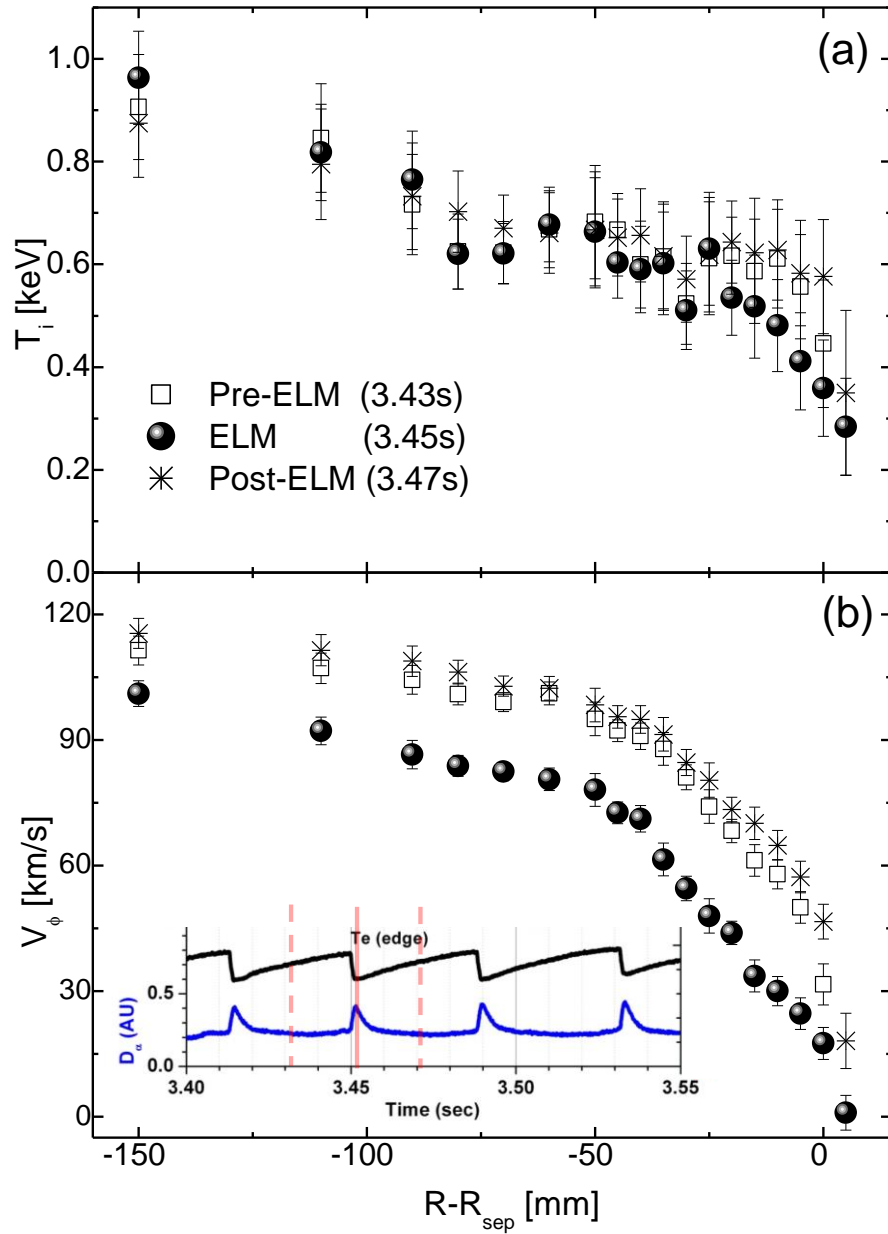
Figure 5. The pedestal profiles evolution before, during and after the ELM crash.
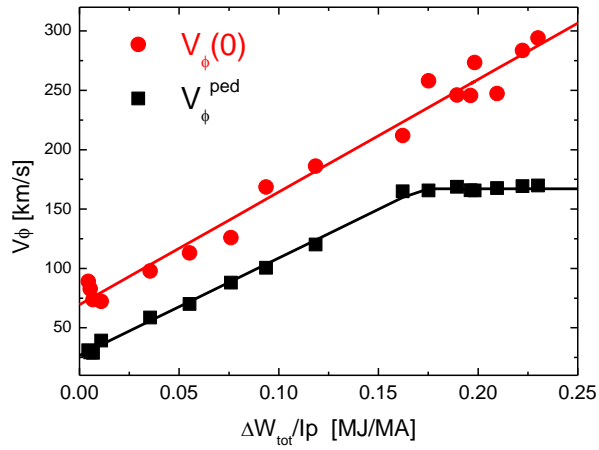
Figure 6. Core and pedestal rotations vs. the increment of the stored energy during L to H transition. The latter is divided by the total plasma current. Note that the rotation pedestal saturates, while the core value increases linearly.
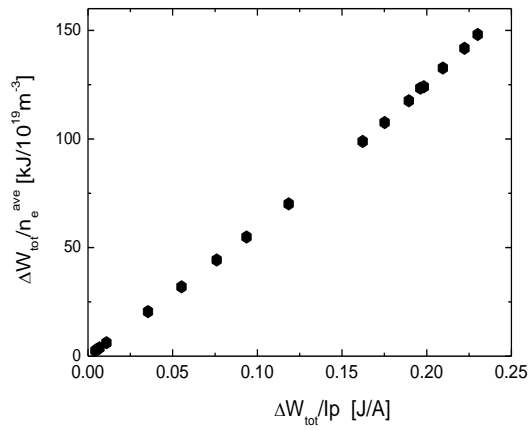
Figure 7. The correlation of the increment of the stored energies divided by the average density and total plasma current.
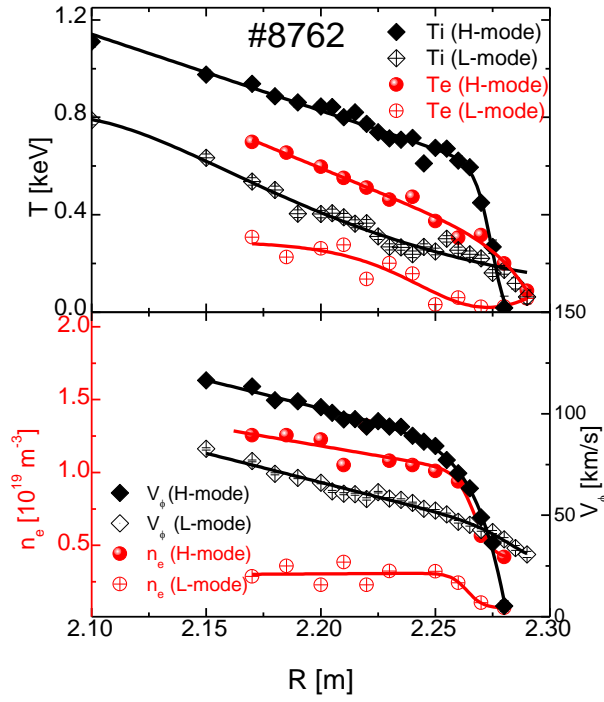
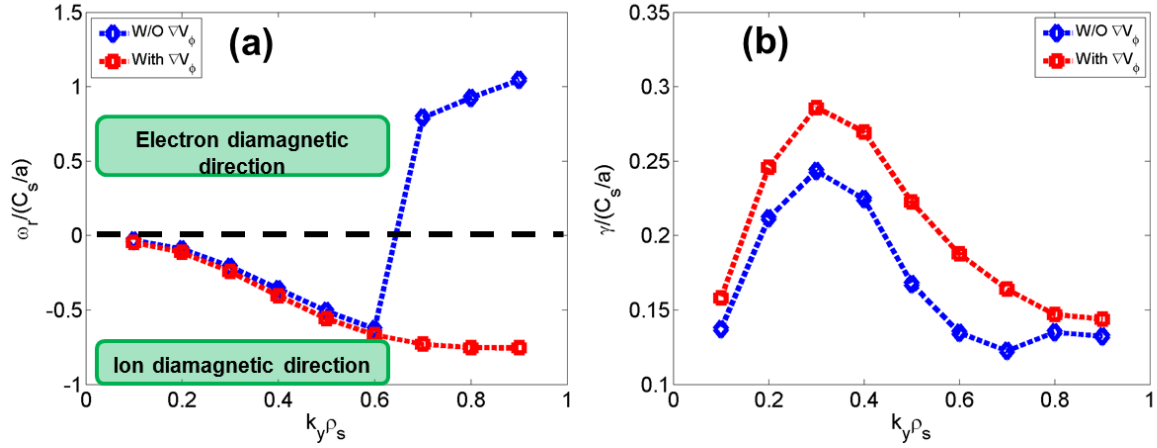Figure 8. All edge pedestal profiles used in linear micro-instability analysis

Figure 9. Gyrokinetic linear stability analysis for the KSTAR H-mode pedestal of #8762. The frequencies (a) and growth rates (b) of instabilities are plotted according to $\mathbf{k_\theta\rho_s}$. The changes of the frequency and growth rate with and w/o $\mathbf{\nabla V_\phi}$ are shown. $\mathbf{a/L_{T_i}} = \mathbf{5.60}$, $\mathbf{a/L_{T_e}} = \mathbf{3.86}$, $\mathbf{a/L_{n_e}} = \mathbf{2.66}$ and $\mathbf{\nabla V_\phi/(C_s/a)} = \mathbf{2.69}$ are parameters in the pedestal.
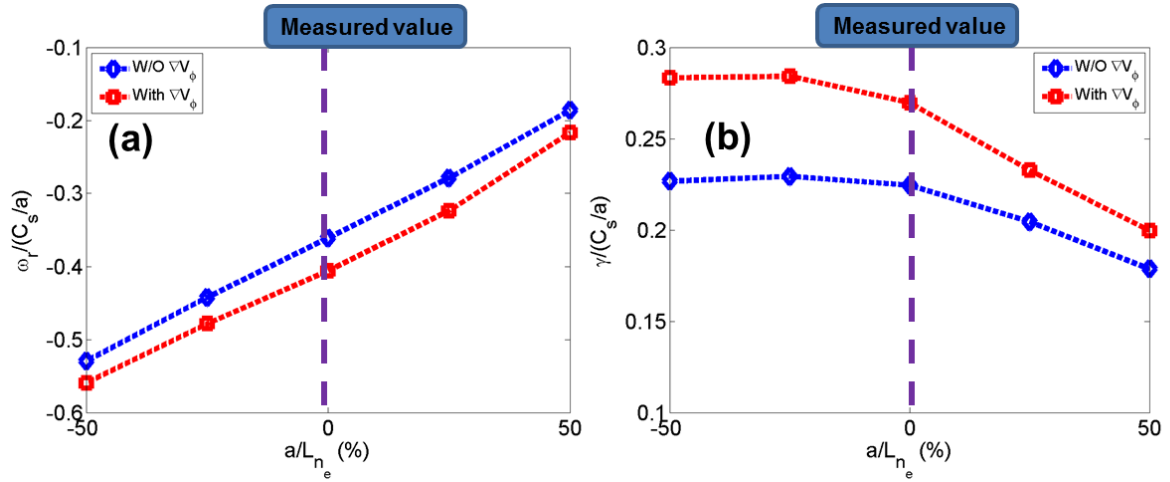
14

Figure 10. Density gradient sensitivity study by gyrokinetic linear stability analysis on the KSTAR H-mode pedestal of #8762. The frequencies (a) and growth rates(b) of instabilities are plotted for a fixed $k_\theta \rho_s = 0.4$. The measured value is $a/L_{n_e} = 2.66$, 50% increase corresponds to $a/L_{n_e} = 3.99$ ($\eta_i = 1.4$), and 50% decrease corresponds to $a/L_{n_e} = 1.33$ ($\eta_i = 4.21$).
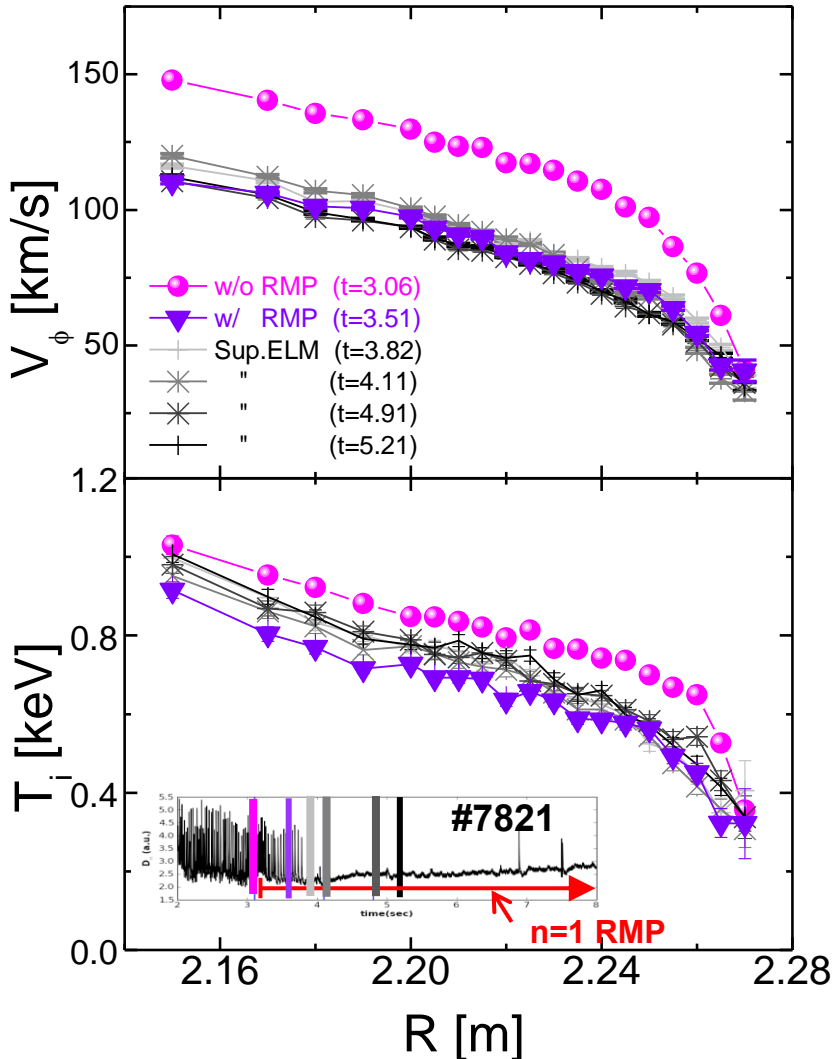

15

Figure 11. The V_ϕ and Ti pedestal tops drop (solid circle) when RMP is turned on, and show little changes during ELM suppression phase.
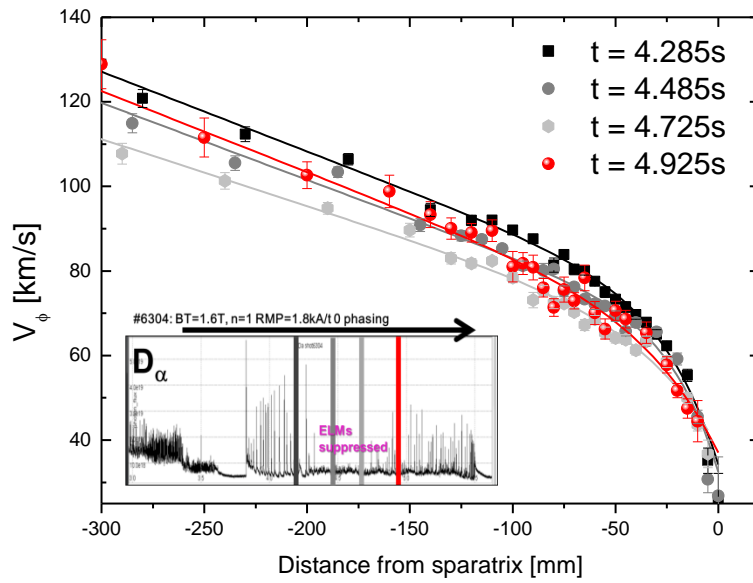

Figure 12. The top values of V_ϕ and Ti pedestal recover their original profiles when RMP is turned off and ELMs reappear.